nature
SUPPLEMENTARY INFORMATION
https://doi.org/10.1038/s41586-019-1334-9
In the format provided by the authors and unedited.

Tracking the precession of single nuclear spins by weak measurements

K. S. Cujia[1], J. M. Boss[1], K. Herb[1], J. Zopes[1] & C. L. Degen[1]*

[1]Department of Physics, ETH Zurich, Zurich, Switzerland. *e-mail: degenc@ethz.ch

Supplementary Information

for the manuscript

"Tracking the precession of a single nuclear spin by weak measurements"

K. S. Cujia, J. M. Boss, K. Herb, J. Zopes, and C. L. Degen

Department of Physics, ETH Zurich, Otto Stern Weg 1, 8093 Zurich, Switzerland

Supplementary Note 1: Derivation of Measurement Back-action

To verify the simple Bloch vector picture of nuclear spin evolution, we calculate the quantum mechanical evolution of the coupled electron-nuclear system. We consider an ideal, closed two-spin system and neglect relaxation due to environmental couplings. The Hamiltonian of the coupled system, in the rotating frame of the electronic spin, is given by

$$\hat{H} = -\gamma_n \mathbf{B} \cdot \hat{\mathbf{I}} + \hat{\mathbf{S}} \cdot \mathbf{A} \cdot \hat{\mathbf{I}} \tag{S1}$$

Here, $\hat{\mathbf{S}}$ and $\hat{\mathbf{I}}$ are the vectors containing the electron and nuclear spin operators, respectively, γ_n is the nuclear gyromagnetic ratio, $\mathbf{B}$ is the external bias field, and $\mathbf{A}$ is the hyperfine tensor. Although in our experiments the electronic spin is $S = 1$, we always work with the $m_S = 0$ and $m_S = -1$ spin-sublevels (whose transition energy is well separated from the $m_S = 0$ to $m_S = +1$ transition) that form an effective spin-1/2 system. Furthermore, assuming weak coupling between the electron and nuclear spins, we apply the secular approximation, leading to the Hamiltonian

$$\hat{H} = \hat{H}_0 + \hat{H}_{int} = -\omega_n \hat{I}_z + a_\parallel \left(\hat{S}_e + \hat{S}_z\right) \hat{I}_z + a_\perp \left(\hat{S}_e + \hat{S}_z\right) \hat{I}_x \tag{S2}$$

where $\hat{I}_x = \frac{1}{2}\sigma_x$, $\hat{I}_z = \frac{1}{2}\sigma_z$ and $\hat{S}_z = \frac{1}{2}\left(|0\rangle\langle 0| - |1\rangle\langle 1|\right) = \frac{1}{2}\sigma_z$ are the Pauli spin operators and $\hat{I}_e = \hat{S}_e = \frac{1}{2}\left(|0\rangle\langle 0| + |1\rangle\langle 1|\right)$ are the identities. Before we proceed, we recall the Hausdorff formula for unitary propagation of the density matrix,

$$\hat{U}\hat{\rho}\hat{U}^\dagger = e^{-i\hat{P}t}\hat{\rho}\, e^{i\hat{P}t} = \hat{\rho}\cos(\sqrt{k}t) - \frac{i}{\sqrt{k}}\hat{Q}\sin(\sqrt{k}t) \tag{S3}$$

where $\hat{P}$ and $\hat{Q}$ are operators, k is a scalar, and where $[\hat{P}, \hat{\rho}] = \hat{Q}$ and $[\hat{P}, \hat{Q}] = k\hat{\rho}$.

We now calculate the effect of the first weak measurement. Starting with the sensor (electron) spin in the $|0\rangle$ state and the nuclear spin in the $|x\rangle$ state,

$$\hat{\rho} = \hat{\rho}_{s0} \otimes \hat{\rho}_{n0} = \left(\hat{S}_e + \hat{S}_z\right)\left(\hat{I}_e + \hat{I}_x\right) \tag{S4}$$

We first apply a $\pi/2$ pulse along $\hat{S}_y$,

$$\hat{\rho} = \left(\hat{S}_e + \hat{S}_x\right)\left(\hat{I}_e + \hat{I}_x\right)$$

Next we apply a sequence of N equidistant π pulses spaced by an interpulse delay 2τ. If the delay between the π pulses is adjusted to half the effective nuclear Larmor period, the system evolves under the effective Hamiltonian $g2\hat{S}_z\hat{I}_x$ for a time $t_\beta = N(2\tau)$, where $g = a_\perp/\pi$ is the coupling strength. Evolution under this Hamiltonian generates the conditional rotation around $2\hat{S}_z\hat{I}_x$ with a rotation angle $\beta = gt_\beta = a_\perp t_\beta/\pi$. We call β the *measurement strength*. The corresponding propagator is $U_{N\pi} = \exp(-\beta 2\hat{S}_z\hat{I}_x)$. Using Eq. S3 (with $\hat{P} = \hat{S}_z\hat{I}_x$, $\sqrt{k} = 1/2$), application of the propagator yields

$$\hat{\rho} = \left(\hat{S}_e + \hat{S}_x\cos(\beta) + \hat{S}_y\sin(\beta)\right)\left(\hat{I}_e + \hat{I}_x\right)$$

Applying the second $\pi/2$ pulse along $\hat{S}_x$ we obtain

$$\hat{\rho} = \left(\hat{S}_e + \hat{S}_x\cos(\beta) + \hat{S}_z\sin(\beta)\right)\left(\hat{I}_e + \hat{I}_x\right)$$

Finally we perform a projective (optical) readout of the electronic spin. The optical readout measures $\langle \hat{S}_z \rangle = \mathrm{Tr}\left(\hat{\rho}\hat{S}_z\right) = \sin(\beta)/2$ and re-polarizes the sensor back on to the initial state $\hat{\rho}_{s0}$. We calculate the resulting nuclear state by tracing over the sensor spin,

$$\hat{\rho}_{n0} = \mathrm{Tr}_e\left(\hat{\rho}\right) = \left(\hat{I}_e + \hat{I}_x\right) \tag{S5}$$

We therefore conclude that a nuclear spin in the $|x\rangle$ state is insensitive to a weak measurement.

Nuclear precession now takes place under $\hat{H}_0 = -\omega_n \hat{I}_z$ (Eq. S2) for a time t_s, leading to a mixing of the $\hat{I}_x$ and $\hat{I}_y$ amplitudes,

$$\hat{\rho} = \left(\hat{S}_e + \hat{S}_z\right)\left(\hat{I}_e + \hat{I}_x \cos(\omega_n t_\mathrm{s}) + \hat{I}_y \sin(\omega_n t_\mathrm{s})\right) \tag{S6}$$

Using Eq. S3 and the following commutators, we calculate the outcome of the next weak measurement,

$$\begin{aligned}
\left[\hat{S}_z\hat{I}_x,\, \hat{S}_x\left(\hat{I}_e + a\hat{I}_x\right)\right] &= i\frac{1}{2}\hat{S}_y\left(a\hat{I}_e + \hat{I}_x\right)\ ; \sqrt{k} = \frac{1}{2} \\
\left[\hat{S}_z\hat{I}_x,\, \hat{S}_x\hat{I}_y\right] &= \frac{i}{2}\left\{\hat{S}_z, \hat{S}_x\right\}\hat{I}_z = 0\ ; \sqrt{k} = \frac{1}{2} \\
\left[\hat{S}_z\hat{I}_x,\, \hat{S}_e\hat{I}_y\right] &= \frac{i}{2}\hat{S}_z\hat{I}_z\ ; \sqrt{k} = \frac{1}{2}
\end{aligned}$$

The first $\pi/2$ pulse along $\hat{S}_y$ yields

$$\hat{\rho} = \left(\hat{S}_e + \hat{S}_x\right)\left(\hat{I}_e + \hat{I}_x \cos(\omega_n t_\mathrm{s}) + \hat{I}_y \sin(\omega_n t_\mathrm{s})\right)$$

Application of $\hat{U}_{N\pi}$ results in

$$\begin{aligned}
\hat{\rho} = &\left(\hat{S}_e + \hat{S}_x\cos(\beta)\right)\left(\hat{I}_e + \hat{I}_x\cos(\omega_n t_\mathrm{s})\right) \\
&+ \hat{S}_y\sin(\beta)\left(\hat{I}_e\cos(\omega_n t_\mathrm{s}) + \hat{I}_x\right) \\
&+ \left(\hat{S}_e\cos(\beta) + \hat{S}_x\right)\hat{I}_y\sin(\omega_n t_\mathrm{s}) + \hat{S}_z\hat{I}_z\sin(\omega_n t_\mathrm{s})\sin(\beta)
\end{aligned}$$

The second $\pi/2$ pulse along $\hat{S}_x$ yields

$$\begin{aligned}
\hat{\rho} = &\left(\hat{S}_e + \hat{S}_x\cos(\beta)\right)\left(\hat{I}_e + \hat{I}_x\cos(\omega_n t_\mathrm{s})\right) \\
&+ \hat{S}_z\sin(\beta)\left(\hat{I}_e\cos(\omega_n t_\mathrm{s}) + \hat{I}_x\right) \\
&+ \left(\hat{S}_e\cos(\beta) + \hat{S}_x\right)\hat{I}_y\sin(\omega_n t_\mathrm{s}) - \hat{S}_y\hat{I}_z\sin(\omega_n t_\mathrm{s})\sin(\beta)
\end{aligned} \tag{S7}$$

Optical readout again measures $\langle \hat{S}_z \rangle$ and re-polarizes the sensor back on to the initial state $\hat{\rho}_{s0}$,

$$\langle \hat{S}_z \rangle = \mathrm{Tr}\left(\hat{\rho}\hat{S}_z\right) = \frac{1}{2}\cos(\omega_n t_\mathrm{s})\sin(\beta) \tag{S8}$$

The effect of a single weak measurement now becomes more clear: it maps, proportionally to the measurement strength $\sin(\beta) \approx \beta$, the instantaneous nuclear $\hat{I}_x$ amplitude onto the optically readable $\langle \hat{S}_z \rangle$ component, while only weakly entangling the sensor and nuclear spins $(\sin(\beta)\hat{S}_z\hat{I}_x)$ such that a measurement of $\hat{S}_z$ only partially projects the nuclear spin. The last term in Eq. S7 also indicates that the nuclear $\hat{I}_z$ component develops an oscillatory correlation with the sensor $\hat{S}_y$ component. Since the latter is never measured, the nuclear spin does not experience, on average, a net rotation outside the precession plane. Furthermore, the information about this correlation becomes lost upon optical readout. We again calculate the partially projected nuclear state by tracing over the sensor spin

$$\begin{aligned}\hat{\rho}_{n1} &= \hat{I}_e + \hat{I}_x \cos(\omega_n t_\mathrm{s}) + \hat{I}_y \sin(\omega_n t_\mathrm{s}) \cos(\beta) && \text{(S9)}\\ &= \hat{I}_e + a_1 \hat{I}_x + b_1 \hat{I}_y && \text{(S10)}\end{aligned}$$

where a_1 and b_1 are the respective amplitudes of $\hat{I}_x$ and $\hat{I}_y$. The net effect of a single weak measurement on the nuclear spin is to scale the initial $\hat{I}_y$ amplitude by a factor $\cos(\beta)$.

1. Measurement-induced decoherence

We now apply a series of weak measurements. The next free precession period will again mix the $\hat{I}_x$ and $\hat{I}_y$ amplitudes

$$\begin{aligned}\hat{\rho} = &\left(\hat{S}_e + \hat{S}_z\right)\left(\hat{I}_e + (\cos(\omega_n t_\mathrm{s})\cos(\omega_n t_\mathrm{s}) - \sin(\omega_n t_\mathrm{s})\cos(\beta)\sin(\omega_n t_\mathrm{s}))\,\hat{I}_x\right.\\ &\left. + (\cos(\omega_n t_\mathrm{s})\sin(\omega_n t) + \sin(\omega_n t_\mathrm{s})\cos(\beta)\cos(\omega_n t_\mathrm{s}))\,\hat{I}_y\right)\\ = &\left(\hat{S}_e + \hat{S}_z\right)\left(\hat{I}_e + a_2 \hat{I}_x + b_2 \hat{I}_y\right)\end{aligned}$$

and the subsequent weak measurement will again scale the resulting $\hat{I}_y$ amplitude by a factor $\cos(\beta)$. The nuclear state after the n'th readout is

$$\begin{aligned}\hat{\rho}_n(n) &= \hat{I}_e + \hat{I}_x a_n + \hat{I}_y b_n\\ &= \hat{I}_e + \hat{I}_x\,(a_{n-1}\cos(\omega_n t_\mathrm{s}) - b_{n-1}\sin(\omega_n t_\mathrm{s})) && \text{(S11)}\\ &+ \hat{I}_y\,(a_{n-1}\sin(\omega_n t_\mathrm{s}) + b_{n-1}\cos(\omega_n t_\mathrm{s}))\cos(\beta)\end{aligned}$$

with $a_0 = 1$ and $b_0 = 0$. We next develop recursion relations (Eq. S11) for the $\hat{I}_x$ and $\hat{I}_y$ amplitudes

$$\begin{aligned}a_0 &= 1\\ a_1 &= \cos(\omega_n t_\mathrm{s})\\ a_2 &= \cos^2(\omega_n t_\mathrm{s}) - \sin^2(\omega_n t_\mathrm{s})\cos(\beta)\\ &= \frac{1}{2}\cos(\omega_n(2t_\mathrm{s}))(1+\cos(\beta)) + \frac{1}{2}(1-\cos(\beta))\\ a_3 &= \left(\frac{1}{2}\cos(\omega_n(2t_\mathrm{s}))(1+\cos(\beta)) + \frac{1}{2}(1-\cos(\beta))\right)\cos(\omega_n t_\mathrm{s})\\ &- \left(\frac{1}{2}\sin(\omega_n(2t_\mathrm{s}))(1+\cos(\beta))\cos(\beta)\right)\sin(\omega_n t_\mathrm{s})\\ &= \frac{1}{4}\cos(\omega_n(3t_\mathrm{s}))(1+\cos(\beta))^2 + (1-\cos(\beta))\cos(\omega_n t_\mathrm{s})\left(\frac{1}{2} + \frac{1}{4}(1+\cos(\beta))\right)\\ a_4 &= \frac{1}{8}\cos(\omega_n(4t_\mathrm{s}))(1+\cos(\beta))^3 + (1-\cos(\beta))\left(\frac{1}{2}\cos(\omega_n(2t_\mathrm{s}))(1+\cos(\beta)) + \frac{1}{8}\left(3+\cos^2(\beta)\right)\right)\\ a_n &= \frac{1}{2^{n-1}}\cos(\omega_n(nt_\mathrm{s}))\,(1+\cos(\beta))^{n-1} + (1-\cos(\beta))f_{an}(\ldots)\end{aligned}$$

$$
\begin{aligned}
b_0 &= 0 \\
b_1 &= \sin(\omega_n t_\mathrm{s})\cos(\beta) \\
b_2 &= \cos(\omega_n t_\mathrm{s})\sin(\omega_n t_\mathrm{s})(1+\cos(\beta))\cos(\beta) \\
&= \frac{1}{2}\sin(\omega_n(2t_\mathrm{s}))(1+\cos(\beta))\cos(\beta) \\
b_3 &= \left(\frac{1}{2}\cos(\omega_n(2t_\mathrm{s}))(1+\cos(\beta)) + \frac{1}{2}(1-\cos(\beta))\right)\sin(\omega_n t_\mathrm{s})\cos(\beta) \\
&+ \left(\frac{1}{2}\sin(\omega_n(2t_\mathrm{s}))(1+\cos(\beta))\cos(\beta)\right)\cos(\omega_n t_\mathrm{s})\cos(\beta) \\
&= \frac{1}{4}\sin(\omega_n(3t_\mathrm{s}))\cos(\beta)\,(1+\cos(\beta))^2 + (1-\cos(\beta))\cos(\beta)\sin(\omega_n t_\mathrm{s})\left(\frac{1}{2}-\frac{1}{4}(1+\cos(\beta))\right) \\
b_4 &= \frac{1}{8}\sin(\omega_n(4t_\mathrm{s}))\cos(\beta)(1+\cos(\beta))^3 + \frac{1}{4}(1-\cos(\beta))^2\cos(\beta)(1+\cos(\beta))\sin(\omega_n(2t_\mathrm{s})) \\
b_n &= \frac{1}{2^{n-1}}\sin(\omega_n(nt_\mathrm{s}))\cos(\beta)\,(1+\cos(\beta))^{n-1} + (1-\cos(\beta))f_{bn}(\ldots)
\end{aligned}
$$

where $f_{an,bn}(\ldots)$ are polynomial functions which depend on $\cos(\beta)$ and on the parity of $n \in \mathbb{N}$.

$$
\begin{cases}
f_{an,bn}(\cos(\beta), \cos(\omega_n(2m)t_\mathrm{s})); m \in [0 \ldots n/2]\,, & n \text{ even} \\
f_{an,bn}(\cos(\beta), \cos(\omega_n(2m+1)t_\mathrm{s})); m \in [0 \ldots (n-1)/2]\,, & n \text{ odd.}
\end{cases}
$$

For weak measurements, i.e. $\beta \ll 1$, the polynomials $f_{an,bn}(\ldots) \approx \mathcal{O}(1)$ and $(1-\cos(\beta)) \approx 0 + \mathcal{O}(\beta^2)$. We can therefore approximate the amplitudes as

$$
\begin{aligned}
a_n &\approx \cos(\omega_n(nt_\mathrm{s}))\left(\frac{1+\cos(\beta)}{2}\right)^{n-1} \\
b_n &\approx \sin(\omega_n(nt_\mathrm{s}))\cos(\beta)\left(\frac{1+\cos(\beta)}{2}\right)^{n-1}
\end{aligned}
$$

We observe that both amplitudes correspond to quadratures which oscillate at the precession frequency ω_n and become scaled by a power of $\cos(\beta)$. Expanding $\cos(\beta)$ to second order and using the binomial expansion we find

$$
\left(\frac{1+\cos(\beta)}{2}\right)^{n-1} \approx \left(1-\frac{\beta^2}{4}\right)^m = \sum_{n=0}^{m}\binom{m}{n}(1)^{m-n}(-1)^n\left(\frac{\beta^2}{4}\right)^n
$$

where we have set $m = n-1$. To observe the approximate scaling of this term at the n'th readout, we assume the limit of a large number of readouts m and use Stirling's formula to approximate the factorials

$$
\sum_{n=0}^{m}\binom{m}{n}(1)^{m-n}(-1)^n\left(\frac{\beta^2}{4}\right)^n \approx \sum_{n=0}^{m}\frac{m^n}{n!}(-1)^n\left(\frac{\beta^2}{4}\right)^n = \sum_{n=0}^{m}\frac{1}{n!}\left(\frac{-m\beta^2}{4}\right)^n \approx e^{-m\beta^2/4} \tag{S12}
$$

The scaling for the nuclear state follows the form

$$
\hat{\rho}_n(t) \approx \hat{I}_e + \left(\hat{I}_x\cos(\omega_n t) + \hat{I}_y\sin(\omega_n t)\right)e^{-\Gamma_\beta t} + \mathcal{O}(\beta^2) \tag{S13}
$$

where $t = n \cdot t_\mathrm{s}\,; n \in \mathbb{N}$ with t_s being the sampling period and $\Gamma_\beta = \beta^2/(4t_\mathrm{s})$. For $t \to \infty$, $\hat{\rho}_n \to \hat{I}_e$. Hence, the net effect of a series of weak measurements is an exponential decay of the nuclear coherences $\hat{I}_x$ and $\hat{I}_y$

at a measurement-induced rate Γ_β proportional to the square of the measurement strength, ultimately leading to a fully mixed state. From Eq. S12 we observe that the number of measurements that can be performed before the nuclear spin dephases (defined as a $1/e$ decay) is $n = 4/\beta^2$. Alternatively the dephasing time is

$$T_\beta = \frac{1}{\Gamma_\beta} = \frac{4}{\beta^2} t_\mathrm{s}$$

Any nuclear spin will also have some intrinsic dephasing $\Gamma_0 = (T_{2,n}^*)^{-1}$ given by the intrinsic dephasing time $T_{2,n}^*$. The total decay rate is then the sum of all contributions

$$\Gamma = \Gamma_\beta + \Gamma_0$$

2. Frequency synchronization

We now turn our attention to the validity of our approximations for Eq. S13. We first consider the case when the effective sampling time approximates a half or a full Larmor period. Such a scenario corresponds to the case when we continuously measure the nuclear spin when it finds itself along the X (or Y) axes in the Bloch sphere. We thus go back to Eq. S11 and set

$$\omega_n t_\mathrm{s} = 2\pi \left(\frac{T/2 \pm \delta t}{T}\right) = \pi \pm \frac{2\pi\delta t}{T} = \pi \pm \delta\alpha$$

where T is the Larmor period and $\delta t \ll T$ is the detuning in the sampling period t_s from half a Larmor period. From Eq. S11, the nuclear state at the k_{th} readout becomes

$$\begin{aligned}\hat{\rho}_n(n) &= \hat{I}_e + \Big(\hat{I}_x \left(a_{n-1}\cos(\delta\alpha) - b_{n-1}\sin(\delta\alpha)\right) + \hat{I}_y \left(a_{n-1}\sin(\delta\alpha) + b_{n-1}\cos(\delta\alpha)\right)\cos(\beta)\Big)\cos(\pi) \\ &\approx \hat{I}_e + \left(\hat{I}_x \left(a_{n-1}\left(1 - \frac{\delta\alpha^2}{2}\right) - b_{n-1}\delta\alpha\right) + \hat{I}_y \left(a_{n-1}\delta\alpha + b_{n-1}\left(1 - \frac{\delta\alpha^2}{2}\right)\right)\cos(\beta)\right)\cos(\pi) + \mathcal{O}(\delta\alpha^3)\end{aligned}$$

Developing the recursion for the amplitudes a_n and b_n with $a_0 = 1$ and $b_0 = 0$, we find

$$\begin{aligned}a_0 &= 1 \\ a_1 &= -\left(1 - \frac{\delta\alpha^2}{2}\right) \\ a_2 &= 1 - \delta\alpha^2\left(1 + \cos(\beta)\right) \\ a_3 &= -\left(1 - \delta\alpha^2\left(\frac{1}{2} + (1 + \cos(\beta))^2\right)\right) \\ a_n &= (-1)^n\left(1 - \delta\alpha^2 f_{an}\left(\cos(\beta)\right)\right) + \mathcal{O}(\delta\alpha^3)\end{aligned}$$

$$\begin{aligned}b_0 &= 0 \\ b_1 &= -\delta\alpha\cos(\beta) \\ b_2 &= \delta\alpha\cos(\beta)(1 + \cos(\beta)) \\ b_3 &= -\delta\alpha\cos(\beta)(1 + \cos(\beta)(1 + \cos(\beta))) \\ b_n &= (-1)^n\delta\alpha\cos(\beta) f_{bn}(\cos(\beta)) + \mathcal{O}(\delta\alpha^3)\end{aligned}$$

where $f_{an,bn}$ are polynomial functions of order n on $\cos(\beta)$. The nuclear state is therefore

$$\hat{\rho}_n(n) \approx \hat{I}_e + \Big(\hat{I}_x\left(1 - \delta\alpha^2 f_{an}(\cos(\beta))\right) + \hat{I}_y\left(\delta\alpha\cos(\beta) f_{bn}(\cos(\beta))\right)\Big)\cos(n\pi)$$

as the product $\delta\alpha\cos(\beta) \to 0$, the nuclear state becomes

$$\hat{\rho}_n(n) \approx \hat{I}_e + \hat{I}_x \cos(n\pi) = \hat{I}_e + \hat{I}_x \cos((0.5\omega_s)t_\mathrm{s}) \tag{S14}$$

where $\omega_s = 2\pi t_\mathrm{s}^{-1}$. Eq. (S14) reveals that we effectively observe a state which remains unaffected by the measurements and is precessing at (half) the sampling frequency, and not at its Larmor frequency. For an increasing detuning $\delta\alpha$, we only observe this effect for stronger measurements, *i.e.*, for $\beta \to \pi/2$, where the measurement becomes increasingly projective. In this case, the product $\delta\alpha\cos(\beta) \to 0$ and we approach the behavior of Eq. S14. It is easy to see that for an effective sampling time close to the Larmor period, i.e. $t_\mathrm{s} \approx T$, the behavior is completely analogous and the nuclear state would be

$$\hat{\rho}_n(n) \approx \hat{I}_e + \hat{I}_x \cos(\omega_s t_\mathrm{s}) \tag{S15}$$

3. Nuclear spin z-component

In our analysis we have assumed a nuclear spin with zero $\hat{I}_z$ component. It is nevertheless important to note what the evolution for a finite $\hat{I}_z$ polarization looks like. From Eq. S4 we observe that the presence of a finite nuclear spin $\hat{I}_z$ component right before a measurement leads to an additional term in the system density matrix of the form

$$\propto \left(\hat{S}_e + \hat{S}_x\right)\left(\hat{I}_z\right)$$

To observe the measurement effect on this component, we first calculate the commutators

$$\begin{aligned}\left[\hat{S}_z\hat{I}_x,\, \hat{S}_x\hat{I}_z\right] &= -\frac{i}{2}\left\{\hat{S}_z, \hat{S}_x\right\}\hat{I}_y = 0\\ \left[\hat{S}_z\hat{I}_x,\, \hat{S}_e\hat{I}_z\right] &= -\frac{i}{2}\hat{S}_z\hat{I}_y\end{aligned}$$

The weak measurement transforms this component according to Eq. S3 (with $\sqrt{k} = 1/4$)

$$\propto \left(\hat{S}_e + \hat{S}_x\right)\left(\hat{I}_z\right) \to \hat{S}_e\hat{I}_z\cos(\beta) - \hat{S}_z\hat{I}_y\sin(\beta) + \hat{S}_x\hat{I}_z$$

The second $\pi/2$ pulse on the sensor spin followed by optical readout therefore yield a partially projected nuclear state of the form

$$\hat{S}_e\hat{I}_z\cos(\beta) + \hat{S}_y\hat{I}_y\sin(\beta) + \hat{S}_x\hat{I}_z \to \hat{I}_z\cos(\beta)$$

Larmor precession only rotates the in-plane components, so an $\hat{I}_z$ component of a precessing nuclear spin upon n weak measurements evolves in analogy to its $\hat{I}_y$ component without the effect of Larmor precession.

$$\hat{I}_z\cos(\beta) \to \hat{I}_z\left(\cos(\beta)\right)^n \approx \left(\hat{I}_z\right)e^{-n\beta^2/2}$$

The nuclear $\hat{I}_z$ component therefore experiences a measurement-induced exponential decay at double the rate of the in-plane components. As indicated in Eq. S12, the slower decay rate for in-plane spin components is due to Larmor precession.

Supplementary Note 2: Signal-to-Noise Ratio

We estimate the signal-to-noise ratio (SNR) for the weak measurement protocol of Fig. 1b. For our estimation, we assume that the output noise is dominated by the shot noise of the optical readout (and not by quantum projection noise), which is a typical situation for experiments with NV centers. For a discussion of readout noise vs. quantum projection noise see Ref. [1]. When dominated by shot noise, the SNR per unit time is given by the ratio between the differential photon count δC_{tot} (the signal) and the square root of the total photon counts C_{tot} (the noise), normalized to the total measurement time T_{tot},

$$\mathrm{SNR} = \frac{\delta C_{\mathrm{tot}}}{\sqrt{C_{\mathrm{tot}} T_{\mathrm{tot}}}} \tag{S16}$$

Here, δC_{tot} corresponds to the change in optical intensity that is proportional to the meter spin $\hat{S}_z$ state, and C_{tot} corresponds to the total intensity that determines the shot noise.

Our weak measurement experiment consists of an initialization step that prepares the nuclear spin in the $\hat{I}_x$ state, followed by n weak measurements separated by a sampling time t_{s}. The duration of a single repetition of the experiment is given by

$$T_{\mathrm{tot}} = t_{\mathrm{init}} + n t_{\mathrm{s}} \tag{S17}$$

where t_{init} is the time it takes to initialize the nuclear spin into $\hat{I}_x$. The total counts are given by

$$C_{\mathrm{tot}} = n C_0 \tag{S18}$$

where C_0 is the photon count of one optical readout. The differential photon count (signal amplitude) of the j'th weak measurement is given by

$$\delta C_j = \frac{1}{2}\epsilon C_0 \sin(g t_\beta) e^{-\Gamma_{\mathrm{e}} t_\beta} e^{-j\Gamma'_{\mathrm{n}} t_{\mathrm{s}}} \approx \frac{1}{2}\epsilon C_0 g t_\beta e^{-\Gamma_{\mathrm{e}} t_\beta} e^{-j\Gamma'_{\mathrm{n}} t_{\mathrm{s}}} \tag{S19}$$

where ϵ is the optical intensity contrast, g is the coupling constant, t_β is the interaction time, and $\Gamma_{\mathrm{e}} = 1/T_{2,\mathrm{DD}}$ is the electronic decoherence rate (assumed to be of first order) that is effective during t_β. The approximation $\sin(g t_\beta) \approx g t_\beta \ll \pi/2$ acknowledges that the measurement is weak. Γ'_{n} is the nuclear dephasing rate,

$$\Gamma'_{\mathrm{n}} = \Gamma_{\mathrm{n}} + \Gamma_\beta = \Gamma_{\mathrm{n}} + \frac{g^2 t_\beta^2}{4 t_{\mathrm{s}}} \tag{S20}$$

which is the sum of the intrinsic dephasing rate Γ_{n} and the measurement-induced dephasing rate $\Gamma_\beta = \beta^2/(4t_{\mathrm{s}}) = (g t_\beta)^2/(4 t_{\mathrm{s}})$ (see Supplementary Note 1). The total differential photon count is the sum over all δC_j,

$$\delta C_{\mathrm{tot}} \approx \sum_{j=1}^{n} \delta C_j \approx \frac{\epsilon C_0 g t_\beta e^{-\Gamma_{\mathrm{e}} t_\beta}(1 - e^{-n\Gamma'_{\mathrm{n}} t_{\mathrm{s}}})}{2\Gamma'_{\mathrm{n}} t_{\mathrm{s}}} \tag{S21}$$

where we have replaced the sum by an integral and performed the integration. The SNR is then given by

$$\boxed{\mathrm{SNR}_{\mathrm{weak}} = \frac{\delta C_{\mathrm{tot}}}{\sqrt{C_{\mathrm{tot}} T_{\mathrm{tot}}}} = \frac{\epsilon \sqrt{C_0} g t_\beta e^{-\Gamma_{\mathrm{e}} t_\beta}(1 - e^{-n\Gamma'_{\mathrm{n}} t_{\mathrm{s}}})}{2\Gamma'_{\mathrm{n}} t_{\mathrm{s}} \sqrt{n(t_{\mathrm{init}} + n t_{\mathrm{s}})}}} \tag{S22}$$

We now simplify this SNR by making the following assumptions:

- The initialization time is similar to (or shorter than) the duration of free precession, $t_{\rm init} \leq n t_{\rm s}$. This assumption is only roughly fulfilled in our experiments. The assumption is justified by the argument that initializing and detecting a nuclear spin will require approximately the same time, since governed by the same coupling constant.
- The sensor readout/reset time $t_{\rm d}$ is short compared to the interrogation time t_β, such that $t_{\rm s} = t_\beta + t_{\rm d} \approx t_\beta$. This assumption is not always met in our experiments, but will in general hold for weak couplings, which is the most important scenario.

The simplified SNR is

$$\mathrm{SNR}_{\rm weak} \approx \frac{1}{2}\epsilon\sqrt{C_0} g e^{-\Gamma_{\rm e} t_\beta} \frac{1 - e^{-n\Gamma_{\rm n}' t_\beta}}{n\Gamma_{\rm n}' \sqrt{t_\beta}} \tag{S23}$$

The two free experimental parameters in this SNR are the number of measurements n and the interaction time t_β. To ensure a spectral resolution on the order of the nuclear linewidth, the duration of the time trace must be at least as long as the nuclear dephasing time $T_{2,\rm n}^*$,

$$n \geq \frac{T_{2,\rm n}^*}{t_{\rm s}} \approx \frac{1}{\Gamma_{\rm n} t_\beta} \tag{S24}$$

To choose an interaction time t_β, we impose that the measurement-induced dephasing rate Γ_β is less than the intrinsic dephasing rate $\Gamma_{\rm n}$,

$$t_\beta \leq \frac{4\Gamma_{\rm n}}{g^2} \tag{S25}$$

The maximum possible t_β is thereby limited to $T_{2,\rm DD} = 1/\Gamma_{\rm e}$ by the exponential decoherence term $e^{-\Gamma_{\rm e} t_\beta}$, which kicks in once couplings become very weak, $g \lesssim \sqrt{\Gamma_{\rm n}\Gamma_{\rm e}}$. Evaluation of Eqs. (S23-S25) then yields the optimum SNR (up to a factor of order unity)

$$\boxed{\mathrm{SNR}_{\rm weak}^{\rm (opt)} \approx \begin{cases} \epsilon\sqrt{C_0\Gamma_{\rm n}} & \text{for } g\sqrt{T_{2,\rm n}^* T_{2,\rm DD}} > 1 \\ \epsilon\sqrt{C_0\Gamma_{\rm n}} \times g\sqrt{T_{2,\rm n}^* T_{2,\rm DD}} & \text{for } g\sqrt{T_{2,\rm n}^* T_{2,\rm DD}} < 1 \end{cases}} \tag{S26}$$

Since the nuclear dephasing time $T_{2,\rm n}^*$ is typically much longer than $T_{2,\rm DD}$, or can be made long by suitable NMR decoupling sequences, weak measurements allow maintaining a constant SNR beyond the decoherence time $T_{2,\rm DD}$ of the sensor spin, up to an evolution time of approximately $\sqrt{T_{2,\rm n}^* T_{2,\rm DD}}$. This renders weak measurement spectroscopy particularly useful for the detection of very weakly coupled nuclear spins. A qualitative plot of the SNR vs. coupling parameter g, along with curves for the spectral resolution and receiver bandwidth, is given in Extended Data Fig. 7.

Supplementary Data 1: Experimental Parameters

Parameters of NV centers and ^{13}C nuclear spins

NV	g (2π kHz)	$a_{\parallel}$ (2π kHz)	$a_{\perp}$ (2π kHz)	$T_{2,\mathrm{DD}}$ (μs)
1	46.78	-18.61	146.35	42
2	4.651	0.540	14.61	165
3	54.22	16.78	150.75	21
4	33.41	381.21	113.29	35
5	37.18	41.56	117.53	500
6	44.25	99.40	139.1	130
7 (^{13}C $_1$)	6.693	-173.5	20.18	216
7 (^{13}C $_2$)	n/m	49.7	n/m	216
7 (^{13}C $_3$)	19.92	98	63.25	216

TABLE S1: Hyperfine coupling parameters calculated for the nuclear spins associated to each NV center. Following Ref. [2], the parallel coupling $a_{\parallel}$ is determined from a free precession experiment yielding two frequencies whose difference is approximately $a_{\parallel}$. The transverse coupling $a_{\perp}$ is obtained by driving a nuclear Rabi oscillation via the electronic spin, and recording the oscillation frequency f_R, where $a_{\perp}/(2\pi) \approx \pi f_R$. We extract these frequencies from the measurements shown in Fig. S1 to Fig. S11. n/m, not measured.

Parameters for Figures 2

NV center	1
B field	$191.8\,\mathrm{mT}$
NV initialization laser pulse	1.5 μs
NV readout laser pulse	1.5 μs
$\pi/2$ rotation CPMG pulses	24
$\pi/2$ rotation CPMG duration	5.908 μs
Weak measurement CPMG pulses K	$\{1, 2, 4, 6, 8, 12, 16\}$
Weak measurement CPMG duration t_β	$\{0.246, 0.493, 0.985, 1.477, 1.969, 2.954, 3.938\}$ μs
Sampling period t_s	$\{3.24, 3.24, 3.76, 4.24, 5.00, 5.72, 7.20\}$ μs
Number of weak measurements n	61
Integration time	$\{1496, 691, 661, 628, 675, 481, 391\}$ sec
Number of Repetitions	$\{3.798, 1.754, 1.592, 1.444, 1.448, 0.970, 0.703\} \cdot 10^6$

Parameters for Figures 3

Figure 3a	
NV center	3
B field	$190.8\,\mathrm{mT}$
NV initialization laser pulse	$1.5\ \mu$s
NV readout laser pulse	$1.5\ \mu$s
$\pi/2$ rotation CPMG pulses	24
$\pi/2$ rotation CPMG duration	$5.874\ \mu$s
Weak measurement CPMG pulses K	2
Weak measurement CPMG duration t_β	$0.489\ \mu$s
Sampling period t_s	$(3.56 + j\ 0.01)\ \mu\mathrm{s};\ j \in \mathbb{N} = [0, 49]$
Number of weak measurements n	51

Figure 3b,c	
NV center	5
B field	$194\,\mathrm{mT}$
NV initialization laser pulse	$1.5\ \mu$s
NV readout laser pulse	$1.5\ \mu$s
$\pi/2$ rotation CPMG pulses	32
$\pi/2$ rotation CPMG duration	$7.579\ \mu$s
Weak measurement CPMG pulses K	$\{2, 6, 12\}$
Weak measurement CPMG duration t_β	$\{0.474, 1.422, 2.844\}\ \mu$s
Sampling period t_s	$\{3.061, 4.013, 4.956\} + j\ 0.002\ \mu\mathrm{s};\ j \in \mathbb{N} = [0, 48]$
Number of weak measurements n	49

Figure 3d	
NV center	5
B field	$194\,\mathrm{mT}$
NV initialization laser pulse	$1.5\ \mu$s
NV readout laser pulse	$1.5\ \mu$s
$\pi/2$ rotation CPMG pulses	32
$\pi/2$ rotation CPMG duration	$7.579\ \mu$s
Weak measurement CPMG pulses K	12
Weak measurement CPMG duration t_β	$2.844\ \mu$s
Sampling period t_s	$5.933 + j\ 0.001\ \mu\mathrm{s};\ j \in \mathbb{N} = [0, 48]$
Number of weak measurements n	49

Parameters for Figure 4

Figure 4a	
NV center	7
B field	$201.2\,\mathrm{mT}$
NV initialization laser pulse	$1.5\,\mu$s
NV readout laser pulse	$1.5\,\mu$s
CPMG pulses	200
Starting CPMG duration	$222.22\,\mu$s
CPMG duration increments t_s	$0.092\,\mu$s
CPMG harmonic order	5
Number of points n	260

Figure 4b, blue dots	
NV center	7
B field	$201.2\,\mathrm{mT}$
NV initialization laser pulse	$1.5\,\mu$s
NV readout laser pulse	$1.5\,\mu$s
Weak measurement CPMG pulses K	8
Weak measurement CPMG duration t_β	$1.860\,\mu$s
Sampling period t_s	$5.680\,\mu$s
Number of weak measurements n	1520
Contact time for LR-NOVEL	$30\ \mu$s
Ramp amplitude for LR-NOVEL	$10\,\%$
$\pi/2$ rotation RF pulse	$10.903\ \mu$s
Number of polarization repetitions M	1200

Figure 4b, gray dots
See Extended Data Fig. 4,top for experimental parameters

Figure 4 inset	
NV center	2
B field	$190.2\,\mathrm{mT}$
NV initialization laser pulse	$1.5\,\mu$s
NV readout laser pulse	$1.5\,\mu$s
$\pi/2$ rotation CPMG pulses	176
$\pi/2$ rotation CPMG duration	$43.384\,\mu$s
Weak measurement CPMG pulses K	16
Weak measurement CPMG duration t_β	$3.944\,\mu$s
Sampling period t_s	$13.92\,\mu$s
Number of weak measurements n	501

Parameters for Extended Data Figure 2

Extended Data Figure 2	
NV center	4
B field	$190\,\mathrm{mT}$
NV initialization laser pulse	$1.5\,\mu\mathrm{s}$
NV readout laser pulse	$1.5\,\mu\mathrm{s}$
$\pi/2$ rotation CPMG pulses	$\{4, 8, 12, 16, 24, 32\}$
$\pi/2$ rotation CPMG duration	$\{0.822, 1.764, 2.647, 3.523, 5.294, 7.058\}\,\mu\mathrm{s}$
Strong measurement CPMG pulses K	32
Strong measurement CPMG duration t_β	$7.058\,\mu\mathrm{s}$

Parameters for Extended Data Figure 4

Extended Data Figure 4, top	
NV center	7
B field	$201.3\,\mathrm{mT}$
NV initialization laser pulse	$1.5\,\mu\mathrm{s}$
NV readout laser pulse	$1.5\,\mu\mathrm{s}$
Strong measurement CPMG pulses K	120
Strong measurement CPMG duration t_β	$27.899u\,\mu\mathrm{s}$
Sampling period t_s	$8.0\,\mu\mathrm{s}$
Number of points n	500
Contact time for LR-NOVEL	$30\ \mu\mathrm{s}$
Ramp amplitude for LR-NOVEL	$10\,\%$
$\pi/2$ rotation RF pulse	$10.903\ \mu\mathrm{s}$
Number of polarization repetitions M	200

Extended Data Figure 4, bottom	
NV center	7
B field	$201.3\,\mathrm{mT}$
NV initialization laser pulse	$1.5\,\mu\mathrm{s}$
NV readout laser pulse	$1.5\,\mu\mathrm{s}$
Weak measurement CPMG pulses K	16
Weak measurement CPMG duration t_β	$3.720\,\mu\mathrm{s}$
Number of weak measurements n	500
Sampling period t_s	$8.0\,\mu\mathrm{s}$
Contact time for LR-NOVEL	$30\ \mu\mathrm{s}$
Ramp amplitude for LR-NOVEL	$10\,\%$
$\pi/2$ rotation RF pulse	$10.903\ \mu\mathrm{s}$
Number of polarization repetitions M	200

Parameters for Extended Data Figure 5

Extended Data Figure 5a	
NV center	7
B field	$201.3\,\mathrm{mT}$
NV initialization laser pulse	$1.5\,\mu$s
NV readout laser pulse	$1.5\,\mu$s
Weak measurement CPMG pulses K	$\{2, 4, 8, 12, 16\}$
Weak measurement CPMG duration t_β	$\{0.465, 0.930, 1.860, 2.790, 3.720\}\,\mu$s
Number of weak measurements n	800
Sampling period t_s	$8.0\,\mu$s
Contact time for LR-NOVEL	30 μs
Ramp amplitude for LR-NOVEL	$10\,\%$
$\pi/2$ rotation RF pulse	10.903 μs
Number of polarization repetitions M	1200

Extended Data Figure 5b	
NV center	7
B field	$201.3\,\mathrm{mT}$
NV initialization laser pulse	$1.5\,\mu$s
NV readout laser pulse	$1.5\,\mu$s
Weak measurement CPMG pulses K	8
Weak measurement CPMG duration t_β	$1.860\,\mu$s
Number of weak measurements n	800
Sampling period t_s	$8.0\,\mu$s
Contact time for LR-NOVEL	30 μs
Ramp amplitude for LR-NOVEL	$10\,\%$
$\pi/2$ rotation RF pulse	10.903 μs
Number of polarization repetitions M	$\{200, 400, 800, 1200\}$

Extended Data Figure 5c	
NV center	7
B field	$201.3\,\mathrm{mT}$
NV initialization laser pulse	$1.5\,\mu$s
NV readout laser pulse	$1.5\,\mu$s
Weak measurement CPMG pulses K	8
Weak measurement CPMG duration t_β	$1.860\,\mu$s
Number of weak measurements n	800
Sampling period t_s	$8.0\,\mu$s
Contact time for LR-NOVEL	30 μs
Ramp amplitude for LR-NOVEL	$10\,\%$
$\pi/2$ rotation RF pulse	10.903 μs
Number of polarization repetitions M	1200

Supplementary Figures for NV 1

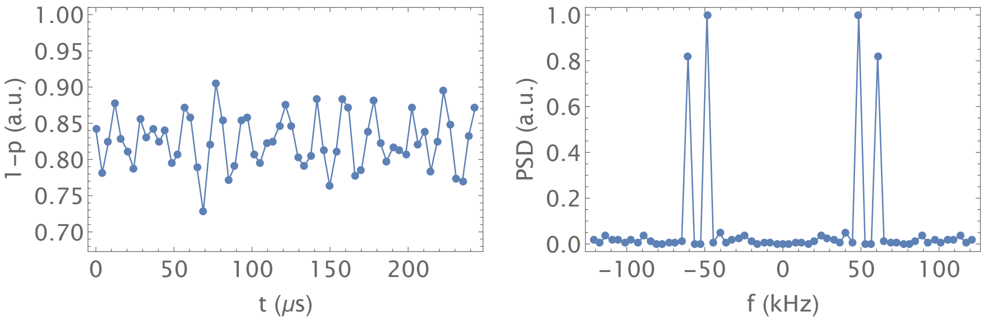

FIG. S1: Correlation spectroscopy for NV1. $t_{\mathrm{s}} = 4.084\,\mu$s.

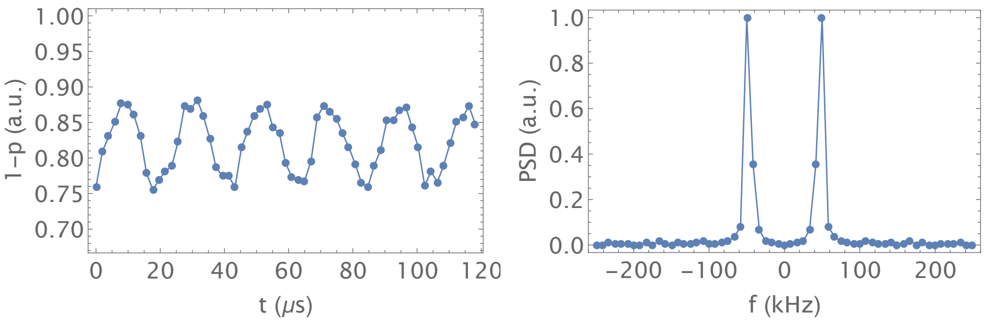

FIG. S2: Correlation spectroscopy with induced nuclear rabi rotation during waiting time for NV1. $t_{\mathrm{s}} = 1.969\,\mu$s.

Supplementary Figures for NV 2

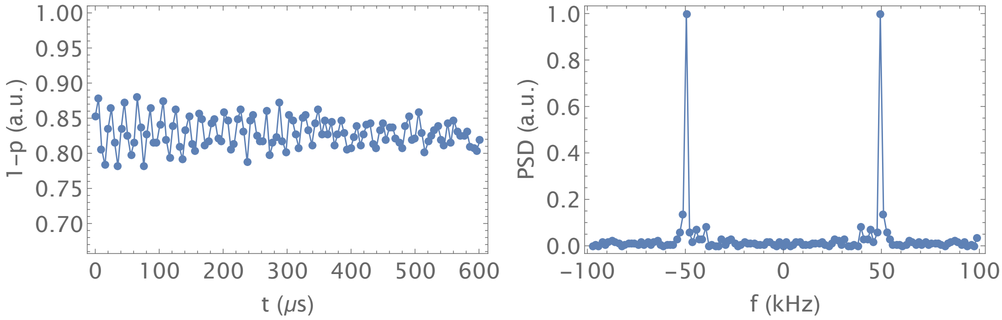

FIG. S3: Correlation spectroscopy for NV2. $t_{\mathrm{s}} = 5.054\,\mu\mathrm{s}$.

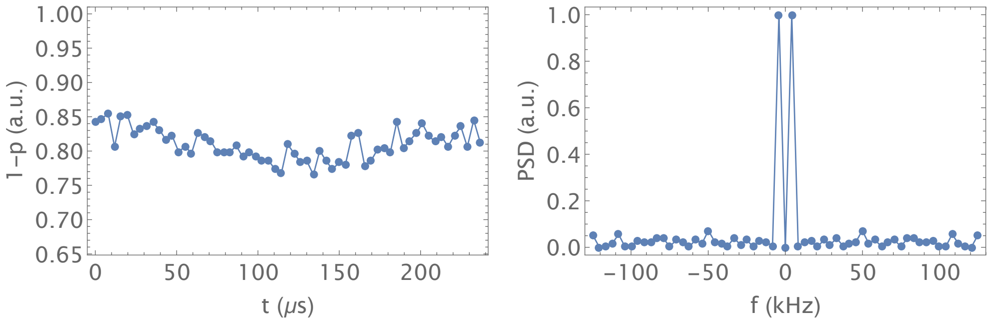

FIG. S4: Correlation spectroscopy with induced nuclear rabi rotation during waiting time for NV2. $t_{\mathrm{s}} = 3.944\,\mu\mathrm{s}$.

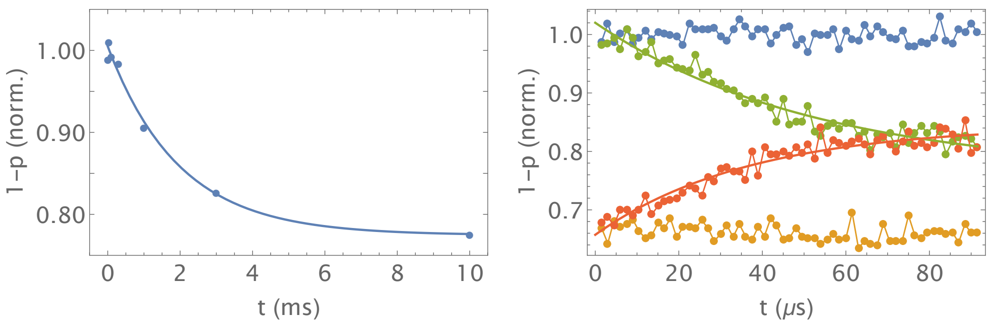

FIG. S5: T_1 relaxation time (left) and T_2 (right). Solid lines are exponential fits yielding $T_1 = 1.97\,\mathrm{ms}$ and $T_{2,\mathrm{echo}} = 52.6\,\mu\mathrm{s}$.

Supplementary Figures for NV 3

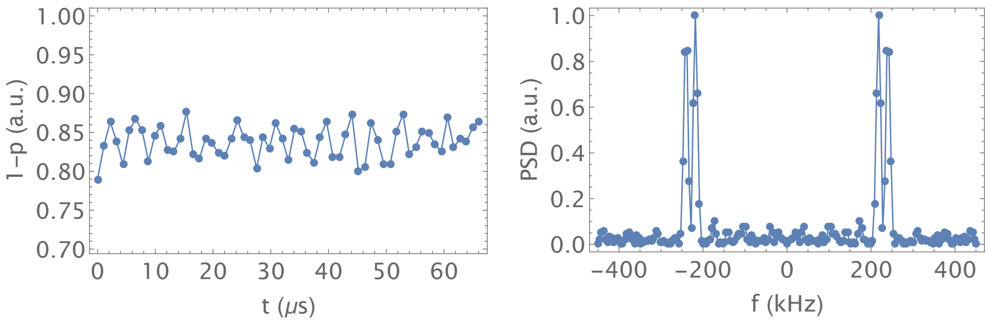

FIG. S6: Correlation spectroscopy for NV3. $t_{\mathrm{s}} = 1.102\,\mu$s.

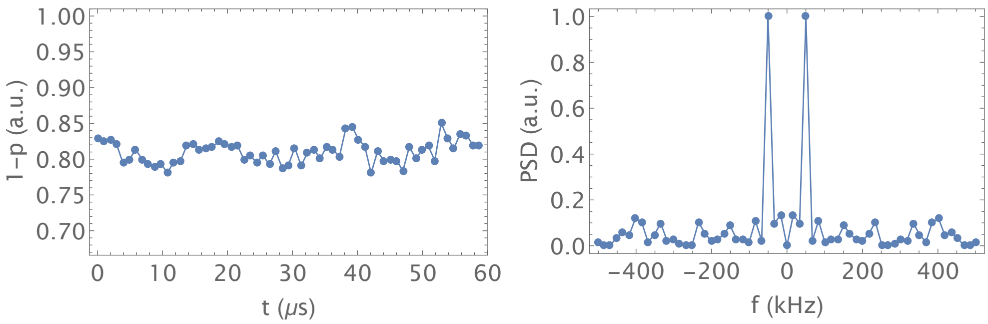

FIG. S7: Correlation spectroscopy with induced nuclear rabi rotation during waiting time for NV3. $t_{\mathrm{s}} = 0.979\,\mu$s.

Supplementary Figures for NV 4

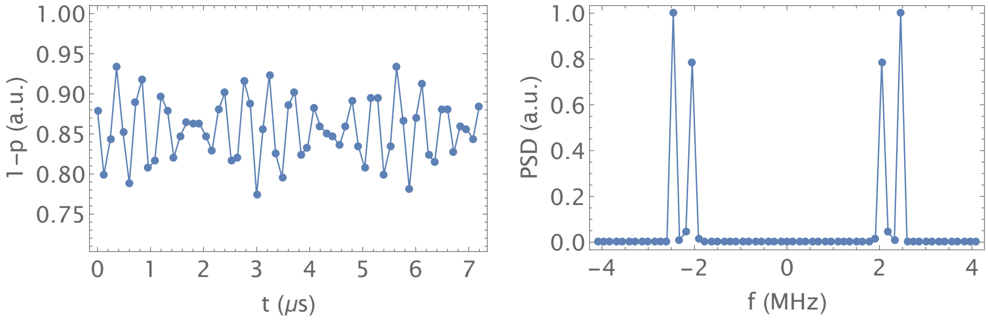

FIG. S8: Correlation spectroscopy for NV4. $t_{\mathrm{s}} = 0.120\,\mu$s.

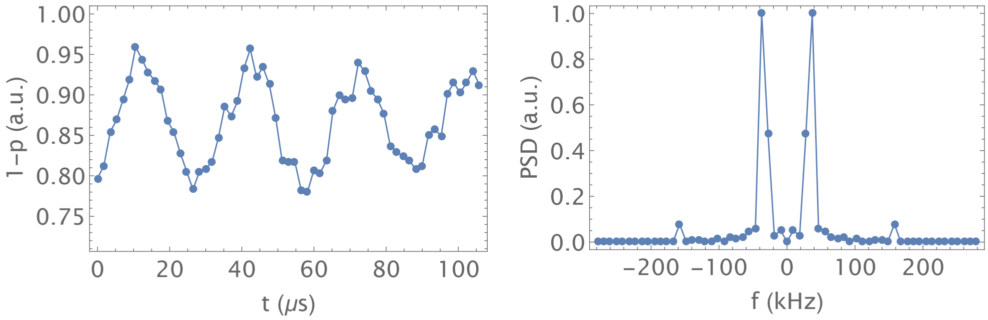

FIG. S9: Correlation spectroscopy with induced nuclear rabi rotation during waiting time for NV4. $t_{\mathrm{s}} = 1.764\,\mu$s.

Supplementary Figures for NV 5

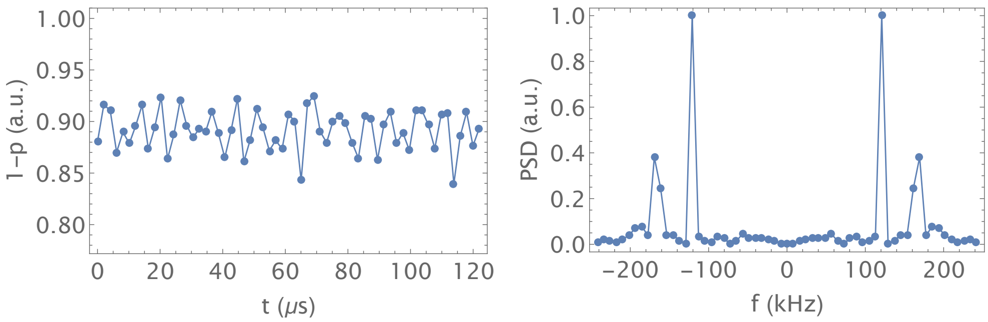

FIG. S10: Correlation spectroscopy for NV5. $t_{\mathrm{s}} = 2.033\,\mu$s.

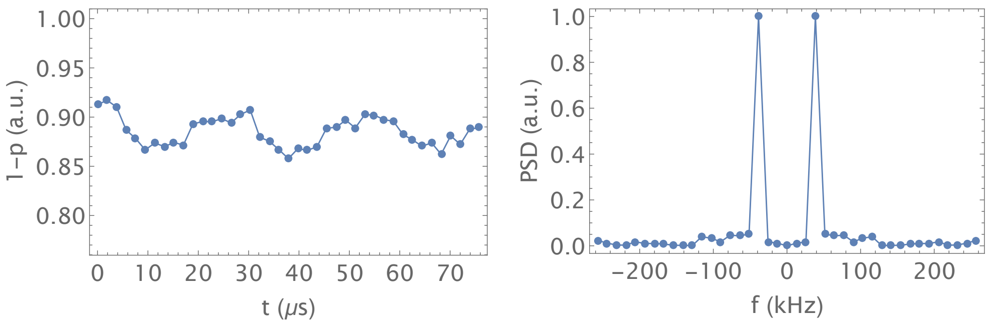

FIG. S11: Correlation spectroscopy with induced nuclear rabi rotation during waiting time for NV5. $t_{\mathrm{s}} = 1.895\,\mu$s.

Supplementary Figures for NV 6

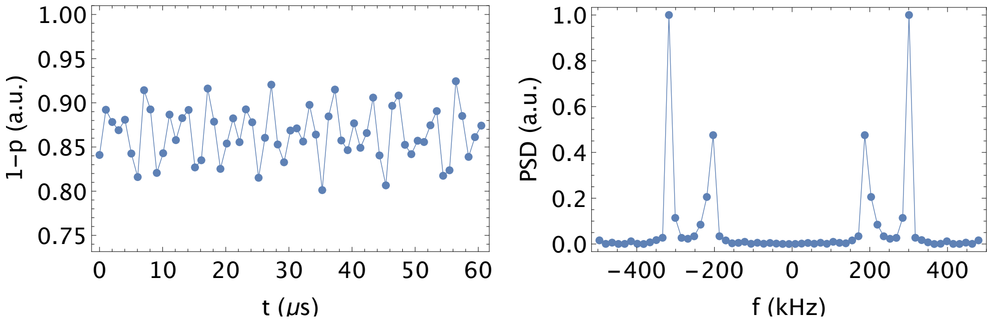

FIG. S12: Correlation spectroscopy for NV5. $t_{\mathrm{s}} = 1.008\,\mu$s.

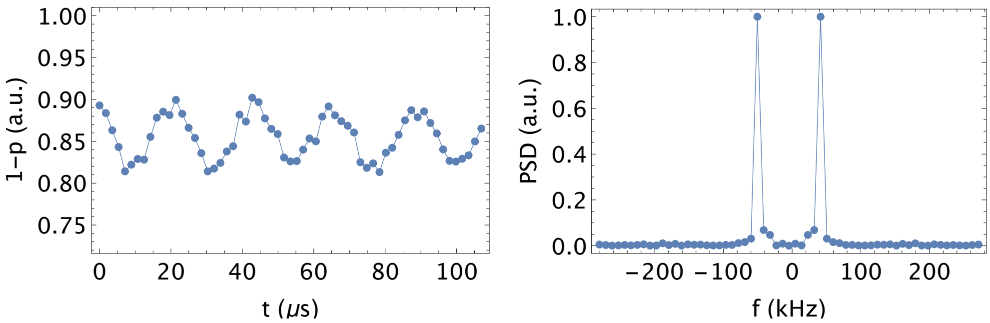

FIG. S13: Correlation spectroscopy with induced nuclear rabi rotation during waiting time for NV5. $t_{\mathrm{s}} = 1.782\,\mu$s.

Supplementary Figures for NV 7

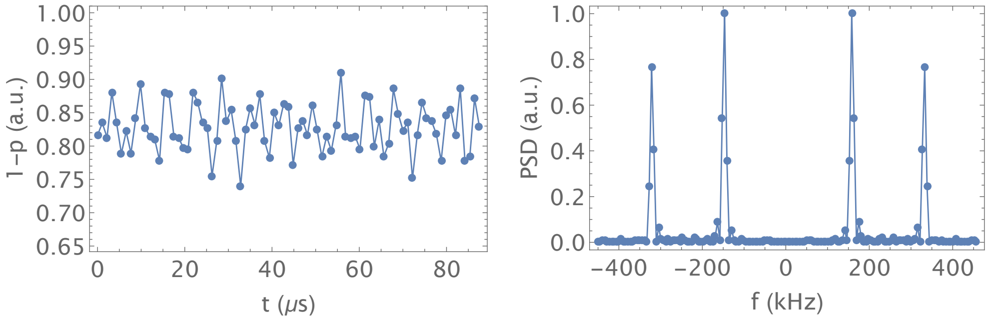

FIG. S14: Correlation spectroscopy for NV7, ^{13}C $_1$. $t_\mathrm{s} = 1.094\,\mu$s.

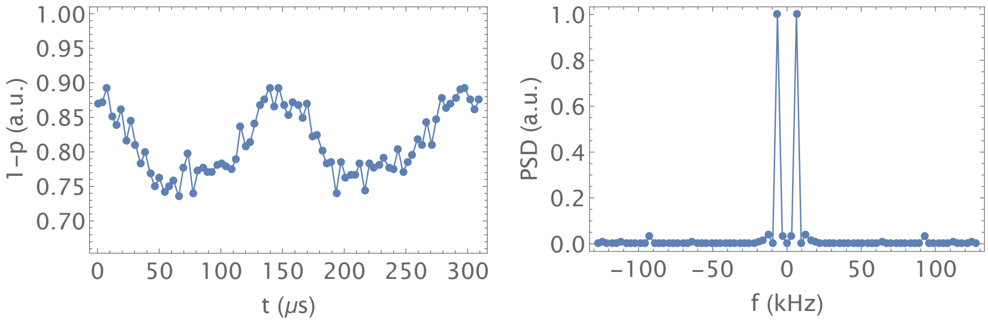

FIG. S15: Correlation spectroscopy with induced nuclear rabi rotation for NV7, ^{13}C $_1$. $t_\mathrm{s} = 3.869\,\mu$s.

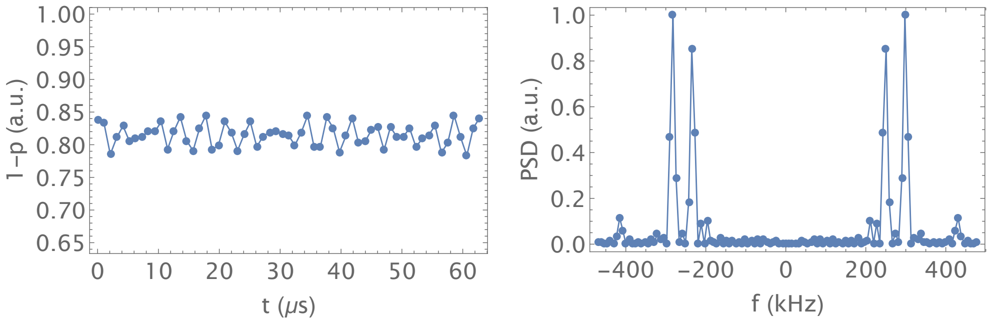

FIG. S16: Correlation spectroscopy for NV7, ^{13}C $_2$. $t_\mathrm{s} = 1.046\,\mu$s.

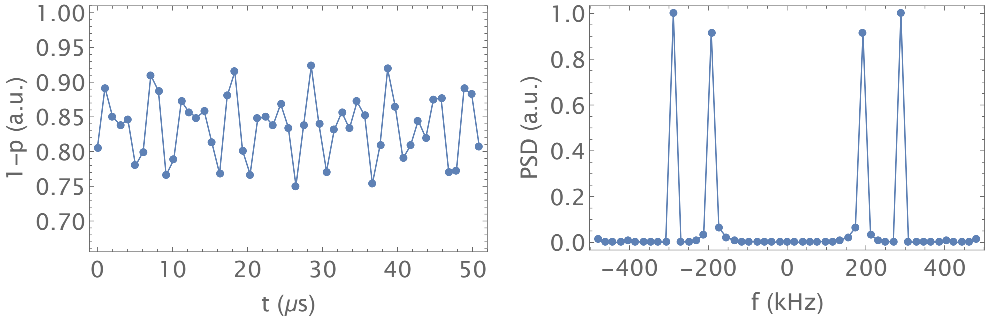

FIG. S17: Correlation spectroscopy for NV7, ^{13}C $_3$. $t_{\mathrm{s}} = 1.018\,\mu$s.

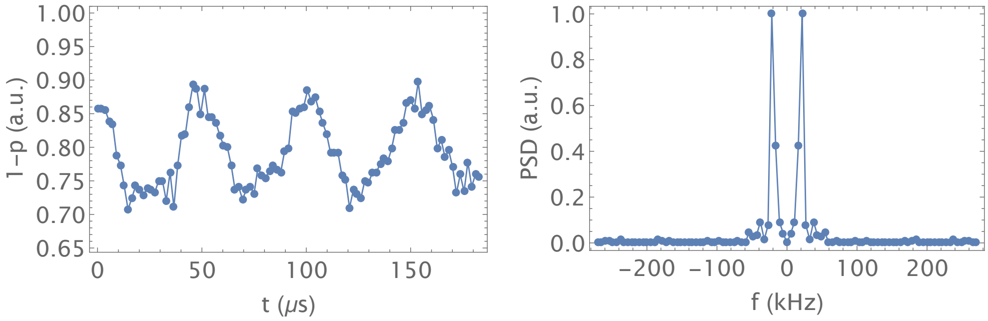

FIG. S18: Correlation spectroscopy with induced nuclear rabi rotation for NV7, ^{13}C $_3$. $t_{\mathrm{s}} = 1.829\,\mu$s.

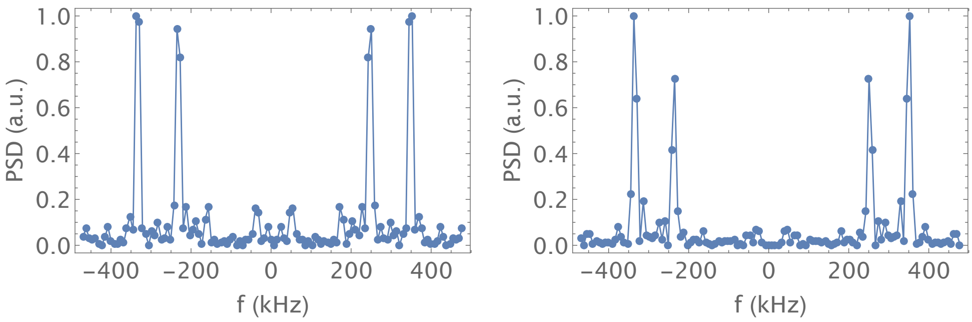

FIG. S19: Correlation spectroscopy for NV7, ^{13}C $_1$. The detection frequency was centered at the position of the 2 peaks associated to ^{13}C $_1$ in Fig. 4a of the main text. $t_{\mathrm{s}} = 1.046\,\mu$s.

References

[1] J. M. Boss, K. S. Cujia, J. Zopes, and C. L. Degen, Science **356**, 837 (2017).
[2] J. M. Boss, K. Chang, J. Armijo, K. Cujia, T. Rosskopf, J. R. Maze, and C. L. Degen, Phys. Rev. Lett. **116**, 197601 (2016).